CHEMISTRY OF MATERIALS

pubs.acs.org/cm

Article

Engineering Highly Fluorescent and Colloidally Stable Blue-Emitting $CsPbBr_3$ Nanoplatelets Using Polysalt/$PbBr_2$ Ligands

Sisi Wang, Wentao Wang, Selin Donmez, Yan Xin, and Hedi Mattoussi*

Cite This: *Chem. Mater.* 2022, 34, 4924−4936

Read Online

ACCESS | Metrics & More | Article Recommendations | Supporting Information

ABSTRACT: Two-dimensional (2D) colloidal perovskite $CsPbBr_3$ nanoplatelets (NPLs) have recently attracted attention as promising blue-emitting materials because of their large exciton binding energy and precisely controlled thickness. However, synthesizing NPLs that are homogeneous and highly fluorescent while exhibiting long-term stability has been challenging, which has limited the successful integration of such materials in optoelectronic devices (e.g., light-emitting devices). Herein, we introduce a strategy relying on surface ligand-engineering, using $PbBr_2$-complexed polymers as coating ligands that impart morphological and colloidal stability while enhancing the photoluminescence quantum yield of perovskite NPLs. The polymers are salt-rich compounds that present several ammonium (or imidazolium) bromide anchoring groups and alkyl chains with different lengths as solubilizing blocks. The presence of quaternary ammonium salts facilitates the dissolution of $PbBr_2$ in organic solutions, forming polysalt-$[Pb_xBr_y]^{2x-y}$ complexes. These complexes strongly interact with the NPLs and eliminate surface defects, compared to the as-grown materials, and improve their structural and morphological stability. This strategy has yielded high-quality blue-emitting NPLs that maintain color purity (with narrow profiles at ∼460 nm) with photoluminescence quantum yield (PLQY) up to 80%. Additionally, significantly enhanced long-term stability of the nanoplatelets under several challenging conditions, including UV irradiation and highly diluted conditions, has been achieved.

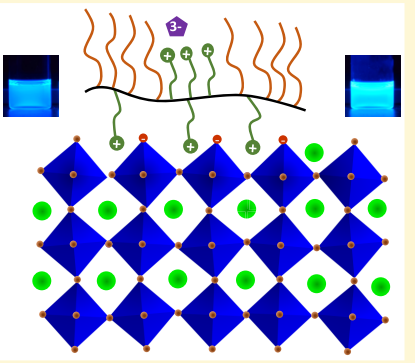

INTRODUCTION

The development of highly efficient semiconductor nanocrystal-based light-emitting diodes (LEDs) has been extensively explored in the last three decades.[1−4] Metal halide perovskite nanocrystals (NCs) are particularly promising for use in next-generation display applications, given their high color purity over a broad range of wavelengths, high photoluminescence quantum yield (PLQY), and easy to implement synthesis.[2,5−10] To this end, balancing the development of the three primary colors to meet the standards of the National Television System Committee (NTSC) is crucial.[11] Although great success has been achieved in fabricating green- and red-emitting perovskite NC-based LEDs, the efficiency of devices emitting in the blue region of the optical spectrum still needs improvements.[2,4] Similar to many other luminescent compounds, developing blue-emitting perovskite materials with high PLQYs and long-term photophysical stability remains difficult to achieve, compared to their green- and red-emitting counterparts. For the latter, samples with near-unity PLQY have been prepared and tested, via either optimization of the growth reaction or postsynthetic passivation of the NC surfaces. Blue-emitting nanocrystals with a high PLQY and long-term stability are still hard to prepare because often these materials tend to exhibit higher density of defects and limited structural stability, as prepared.[8]

Overall, three approaches can be applied to obtain colloidal blue-emitting $CsPbX_3$ NCs: (i) varying the molar fraction of the halide component using mixed Cl^- and Br^- cores; (ii) reducing the size of $CsPbBr_3$ cuboids below the Bohr exciton radius (to ∼2−5 nm), in order to reach the strong carrier confinement regime for these materials; and (iii) growing anisotropic 2D quantum-confined NPLs. However, perovskite NCs with mixed halide cores tend to undergo irreversible phase segregation during operation (e.g., in LED devices), giving rise to color instability.[12,13] Ultra-small $CsPbBr_3$ QDs that can generate blue emission are very difficult to prepare because of the rapid nucleation and growth of these materials. Therefore, reducing the dimensionality of pure bromide-based nanocrystals to below the bulk Bohr exciton radius, by, for example, growing nanoplatelets, offers a promising strategy for shifting the PL to the desired "deep blue" region of the optical spectrum. Because of the strong carrier confinement along the transversal direction, the measured energy band gap strongly depends on the NPL thickness, with larger gap measured for smaller thickness.

Received: January 10, 2022
Revised: April 22, 2022
Published: May 19, 2022

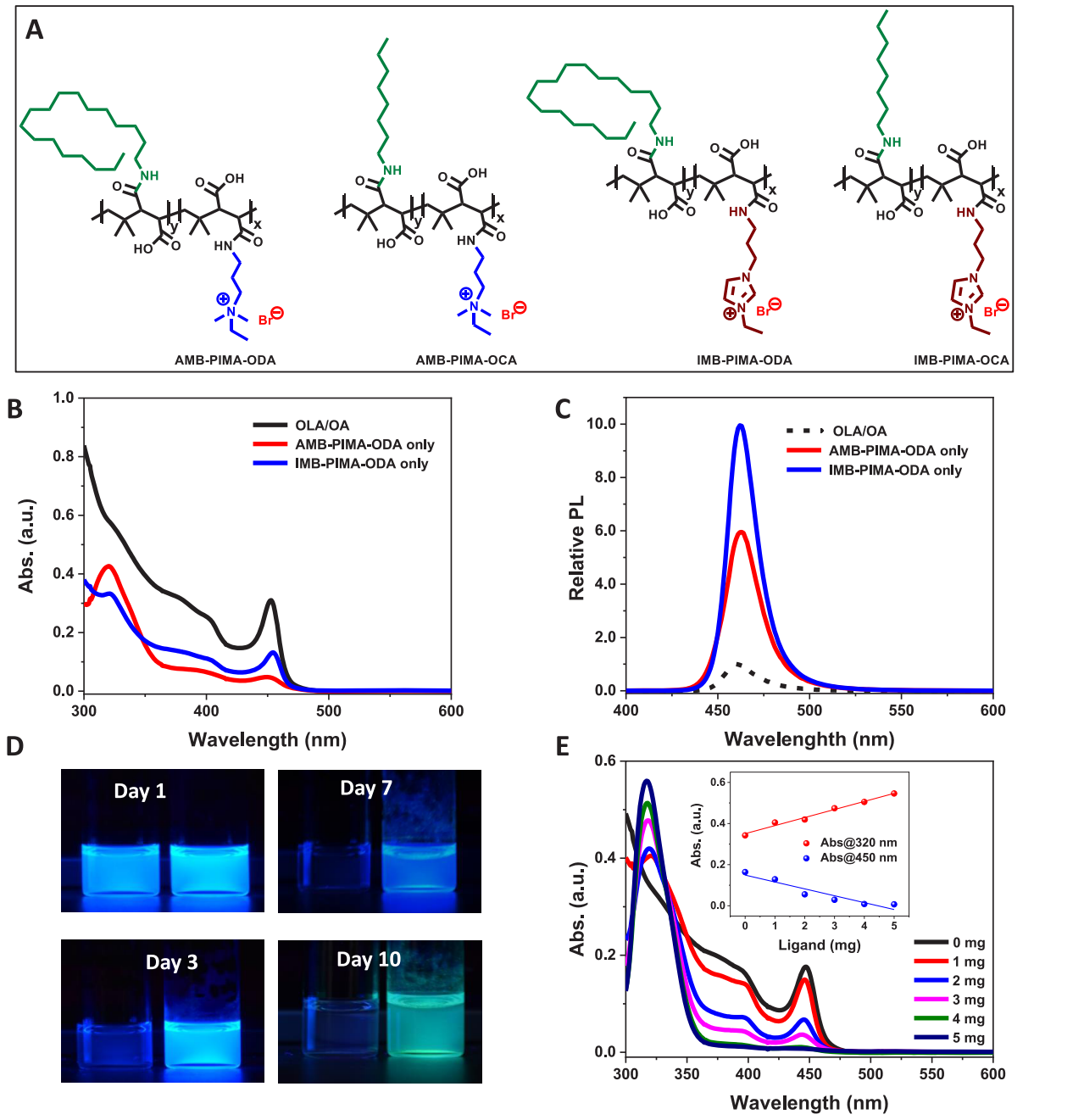

Figure 1. (A) Chemical structures of the polysalt ligands prepared in this work. (B) Changes in the absorption profiles acquired from dispersions of NPLs mixed with polysalts (AMB-PIMA-ODA and IMB-PIMA-ODA) together with the profile measured for OLA/OA-coated nanocrystals shortly after preparation. (C) Relative PL profiles (reported with respect to the native OLA/OA-coated sample) measured for the same dispersions shown in panel B but using concentrations that match at the optical density at 450 nm. (D) Fluorescence images (collected under UV irradiation) from dispersions of NPLs stabilized with AMB-PIMA-ODA and IMB-PIMA-ODA only, tracked over a 10-day period. (E) Changes in the absorption profiles acquired from NPL dispersions mixed with different amounts (in mg) of AMB-PIMA-ODA ligands. The inset shows plots of the optical densities at 450 and 320 nm as a function of the added ligand mass. Reduction in the absorption at the first exciton peak (at 450 nm), due to etching of the NPLs, is coupled to the formation of $[Pb_xBr_y]^{2x-y}$ complexes at 320 nm.

As-grown, NPLs tend to have large numbers of surface defects, which drastically reduce the measured PLQY. In addition, these quasi 2D nanostructures tend to suffer from limited stability. A few groups have tried to address some of these problems by either devising postsynthetic methods to repair the surface defects using $PbBr_2$, or in-situ surface passivation in the presence of excess bromide. Such manipulations were reported to enhance the PLQY of blue-emitting $CsPbBr_3$ NPLs.[8,14−18] Overall, it is agreed on that elimination of the surface bromide vacancies (V_{Br}) plays a key role in enhancing the fluorescence signal, by reducing the nonradiative exciton recombination rates.[19]

As done for the growth of green-emitting $CsPbBr_3$ nanocubes, oleic acid (OA) and oleylamine (OLA) ligands are used for dissolving the organometal precursors and for providing a stabilizing coat of the nanoplatelets. In this strategy, the Cs^+-to-OLA^+ cation molar ratio plays a critical role in reducing the NC thickness down to a few monolayers,

https://doi.org/10.1021/acs.chemmater.2c00082
Chem. Mater. 2022, 34, 4924−4936

to achieve strong carrier confinement.[14,20−22] Those ligands exhibit rather labile interactions with the NC surfaces.[23] The increased surface energy of NPLs combined with the weak binding of the ligands leads to poor colloidal stability under a few relevant conditions, including long-term storage, highly diluted conditions, or when washed with a polar solvent.[24] For instance, the PL profile of $CsPbBr_3$ NPLs shifts from blue (450−465 nm) to green (500−520 nm) with storage time. This change is caused by the rearrangement of the atoms in order to reduce the total surface energy of the NCs, which ultimately results in weaker carrier confinement effects.[25,26] Exploring the use of novel surface capping ligands that can impart better structural stability and more effective electronic passivation of surface defects is very promising. Indeed, a few reports have proven the benefits of this approach. For instance, Li and co-workers have reported that treating NPLs with didodecyldimethyl ammonium bromide (DDAB) post-synthetically increases the dispersion PLQY.[27] Similarly, the groups of Stranks and Tang reported that introducing trioctylphosphine oxide or hexylphosphonic acid (which have stronger binding affinity to perovskite NCs) during the growth reaction yields quantum-confined NPLs with higher PLQY and better stability.[28,29] Despite these findings, progress in achieving effective control over the photophysical and colloidal properties of $CsPbBr_3$ NPLs, through careful manipulation of the surface coating, still lags behind their cuboid counterparts; for the latter, numerous molecular-scale and polymeric coatings have been tested.[30−34] Therefore, developing new capping ligands with stronger binding affinity and better passivation is needed, as this could yield NPLs that exhibit enhanced structural and photophysical stability.

Here, we introduce a new surface engineering strategy, which combines multidentate polymers with salt complexation to achieve structural stability and electronic passivation of $CsPbBr_3$ NPLs. The design of the polysalt-complex ligands builds on previous ideas developed by our group, where polymers presenting multiple alkyl ammonium or imidazolium bromide ion pairs were utilized as electrostatic anchors.[35] Notably, we have found that the new polysalt-complex ligands preserve the anisotropic morphology and crystal structure of the nanoplatelets, while enhancing the PLQY up to ∼80%. In addition, the coating preserves the NPL spectroscopic features under a few key tests, namely, phase transfer between solvents, extended exposure to UV irradiation, and when processed under highly diluted conditions.

RESULTS AND DISCUSSION

The strategy introduced in this report for developing strongly fluorescing, blue-emitting perovskite nanocolloids has been inspired by some of our recent studies.[34,35] Indeed, in two separate studies, we have shown the benefits of using high-affinity, polymer-based ligands that present either multiple zwitterion moieties or salt groups, as binding motifs to impart structural, morphological, and colloidal stability onto $CsPbBr_3$ nanocubes. Whereas the polysalt specifically targets Br^- vacancies for repairing, the poly-sulfobetaine ligands use Lewis acid and Lewis base groups in the zwitterion moieties for coordination onto the NC surface cations and anions simultaneously. Based on those findings, we reasoned that applying Br-based polysalt ligands to $CsPbBr_3$ nanoplatelets would also repair surface vacancies and provide electronic passivation of defect sites, yielding highly fluorescent blue-emitting nanomaterials. The polysalts prepared and tested in this work contain multiple ammonium bromide (AMB) or imidazolium bromide (IMB) ion pairs, as coordinating groups, along with alkyl chains (octylamine, OCA, or octadecylamine, ODA) to promote affinity for organic solvents (see Figure 1A). The ligand synthesis relies on the highly efficient nucleophilic addition reaction between succinic anhydride rings in a poly(isobutylene-alt-maleic anhydride), PIMA, chain and different amine-modified precursors.[35−38] By varying the combination of salt groups and solubilizing blocks, we prepared four different sets of polysalts, namely, AMB-PIMA-ODA, AMB-PMA-OCA, IMB-PIMA-ODA, and IMB-PIMA-OCA. The ligands present 20% AMB/IMB and 80% alkyl chains, where the percentages refer to the molar fraction of salt and alkyl moieties with respect to the number of anhydride monomers per polymer chain. The above stoichiometry corresponds to ∼8 anchors and ∼32 alkyl chains per ligand, respectively.[34,35,37,38]

We first started by testing the ability of the imidazolium- and ammonium-based polysalts to promote PL enhancement while imparting colloidal stability to the NPLs, compared to OLA/OA-stabilized materials. For this, three dispersions were prepared with comparable initial optical densities at the first exciton peak (OD_{450}): one contains OLA/OA−NPLs and two are made of OLA/OA−NPLs mixed with either AMB-PIMA-ODA or IMB-PIMA-ODA. Upon mixing the OLA/OA−NPLs with either AMB-PIMA-ODA or IMB-PIMA-ODA, we observed an instantaneous enhancement in the PL emission, combined with a drop in the absorption at wavelengths above 350 nm and the appearance of a pronounced new absorption feature at ∼320 nm, as summarized in the absorption and PL data shown in Figure 1B,C. However, when tracked for several days, we found that the PL signal progressively decayed with storage time (Figure 1D). The changes in the absorption profiles, namely, the new high energy peak and the reduction in the absorption at 450 nm can be respectively attributed to the simultaneous buildup of $[Pb_xBr_y]^{2x-y}$ complexes, coupled with reduction in the NPL concentration.[39] Such changes imply that etching induced by interactions with the polymer has taken place. Indeed, although highly fluorescent at first, the dispersions become unstable with storage time, resulting in a pronounced decrease in PL and occasional shift to green, as a result of etching (see Figure 1D). To further confirm the decrease in the NPL concentration, we acquired absorption spectra from a set of NPL dispersions, which were mixed with different amounts of polysalts. A pronounced decrease in the NPL excitonic absorption coupled with the buildup of a sizable intensity peak ascribed to the complex at 320 nm was measured (see the inset in Figure 1E). The presence of the isosbestic point indicates that a steady transformation of the NPLs into complex species has taken place.

We attribute the progressive "dissolution" of the NPLs to the strong interaction between the quaternary ammonium/imidazolium groups (along the polymer chain) and $CsPbBr_3$ NPLs. Such interactions result in exfoliation as Cs^+ ions are exchanged with the cationic ammonium, leading to the formation of $[Pb_xBr_y]^{2x-y}$ complexes.[40] This process is dependent on the molar equivalence between ligands and NPLs. Small molar equivalents of ammonium/imidazolium cations provide NCs with enhanced PL, whereas larger molar amounts promote exfoliation via surface cation exchange and the formation of lead halide complexes.[30,40−44] For a given concentration of NPLs, small molar equivalents of the ligand can be introduced to enhance the PL without altering the

https://doi.org/10.1021/acs.chemmater.2c00082
Chem. Mater. 2022, 34, 4924−4936

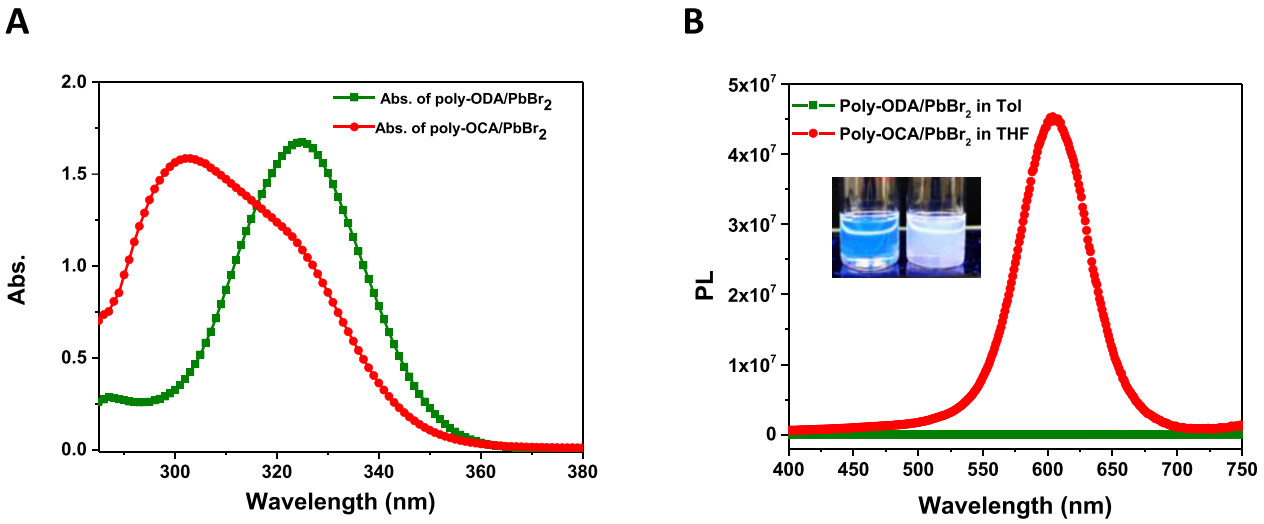

Figure 2. (A) UV absorption spectra and (B) emission profiles acquired from solutions of poly-ODA/$PbBr_2$ complexes in toluene and poly-OCA/$PbBr_2$ complexes in THF. The excitation wavelength for poly-OCA complex in THF is 310 nm while for poly-ODA in toluene, it is 320 nm. The inset in panel B shows the fluorescence images of vials containing poly-ODA/$PbBr_2$ complexes in toluene (left) and poly-OCA/$PbBr_2$ complexes in THF (right), illuminated with a hand-held UV lamp.

integrity of the nanocrystals. However, such an amount would not promote complete substitution of the native ligands and results in only limited colloidal stability.

The rather large longitudinal surface of the anisotropic structures imparts a high surface energy to the NPLs. Thus, interactions with the polysalts promote progressive disintegration of a fraction of the nanoplatelets with likely large number of surface defects. Such transformation is affected by the polysalt concentration and incubation time, as shown in Figure 1D,E. Based on these findings, we reasoned that partially precomplexing the ligands with $PbBr_2$ salt prior to the ligand exchange would promote better structural stability of the NPLs, while also guaranteeing improved photophysical properties. Thus, our approach for ligand substitution first starts with the buildup and characterization of the polysalt/$PbBr_2$ complexes.

Polysalt/$PbBr_2$ Complexation. Initial experiments indicated that dissolution of $PbBr_2$ salt in certain noncoordinating solvents, such as toluene and tetrahydrofuran (THF), is greatly improved in the presence of the polysalt; pure $PbBr_2$ is not soluble in those media.[41,45,46] Dissolution is driven by the complexation reaction between the ammonium bromide or imidazolium bromide and $PbBr_2$ in the solution. For the present case, we used a $PbBr_2$-to-AMB/IMB molar ratio of ~0.7:1, which corresponds to an unsaturated polymer complexation reaction. It has been reported that lead halide complexes in solution exhibit characteristic absorption and emission signatures promoted by ligand-to-metal charge transfer (LMCT).[47,48] Consequently, these features allow one to identify the presence of lead bromide complexes using optical spectroscopy.

Experimental data showed that the polysalt-$PbBr_2$ complexation reactions are solvent-dependent. In particular, when ODA-based polysalts (AMB-PIMA-ODA or IMB-PIMA-ODA) were reacted with $PbBr_2$ in toluene, the measured absorption profile showed a symmetric band centered at ~325 nm, see Figure 2A. In comparison, complexation of $PbBr_2$ with AMB-PIMA-OCA or IMB-PIMA-OCA in THF yielded absorption spectra that show a nonsymmetric broad band with a peak at ~306 nm and a shoulder at ~325 nm, which indicates the coexistence of two different species. In addition, the complex in THF solution exhibits strong-enough emission at ~600 nm to be visually detected, while the polysalt/$PbBr_2$ complexes formed in toluene exhibit negligible emission (see Figure 2B). Based on the literature data, we tentatively assign the species absorbing at ~306 nm to mononuclear $[PbBr_3]^-$, while those absorbing at 325 nm to the polynuclear $[Pb_4Br_{11}]^{3-}$.[39,48,49] The complexation reaction at equilibrium depends on the exact nature of the solvent used. For example, in THF, the following two reactions occur:

$$PbBr_2\,(s) + [Br]^- \rightleftharpoons [PbBr_3]^- \quad (1)$$

$$4PbBr_2\,(s) + 3[Br]^- \rightleftharpoons [Pb_4Br_{11}]^{3-} \quad (2)$$

In contrast, only reaction 2 tends to occur in toluene. We will refer to both complexes as $[Pb_xBr_y]^{2x-y}$. In addition to these results, we found that the complexation reaction also produces trace amounts of white precipitates, which can be attributed to the association of organic compounds (e.g., polymer chains) with lead halide, yielding a hybrid structure such as $L[PbBr_4]^-$. The precipitate exhibits a large absorbance peak at ~357 nm along with a weak broad emission spanning the entire visible spectrum centered at ~620 nm (see Figure S1).[50] In the present study, we have not fully investigated the structure of those compounds, but instead focused on controlling the NPL morphology and fluorescence properties.

Ligand Exchange with Polysalt/$PbBr_2$ and Optical Characterization of the Nanoplatelets. Upon adding the polysalt/$PbBr_2$ complex solution to the NPL dispersion, a strong blue emission, which could be visually detected under ambient lighting, rapidly developed. This provided a first indication that the ligands interact with the NPLs and affect their photophysical properties (see Figure 3B). The mixture was subsequently sonicated for ~2 min and then precipitated using ethyl acetate, to remove the native ligands. The NPLs modified with AMB-PIMA-ODA/$PbBr_2$ or IMB-PIMA-ODA/$PbBr_2$ were readily dispersed in toluene. However, NPLs coated with AMB-PIMA-OCA/$PbBr_2$ or IMB-PIMA-OCA/$PbBr_2$ were phase-transferred to THF instead, as dispersion in toluene could not be implemented. The UV−vis absorption spectra collected from NPLs coated with poly-ODA/$PbBr_2$

https://doi.org/10.1021/acs.chemmater.2c00082
Chem. Mater. 2022, 34, 4924−4936

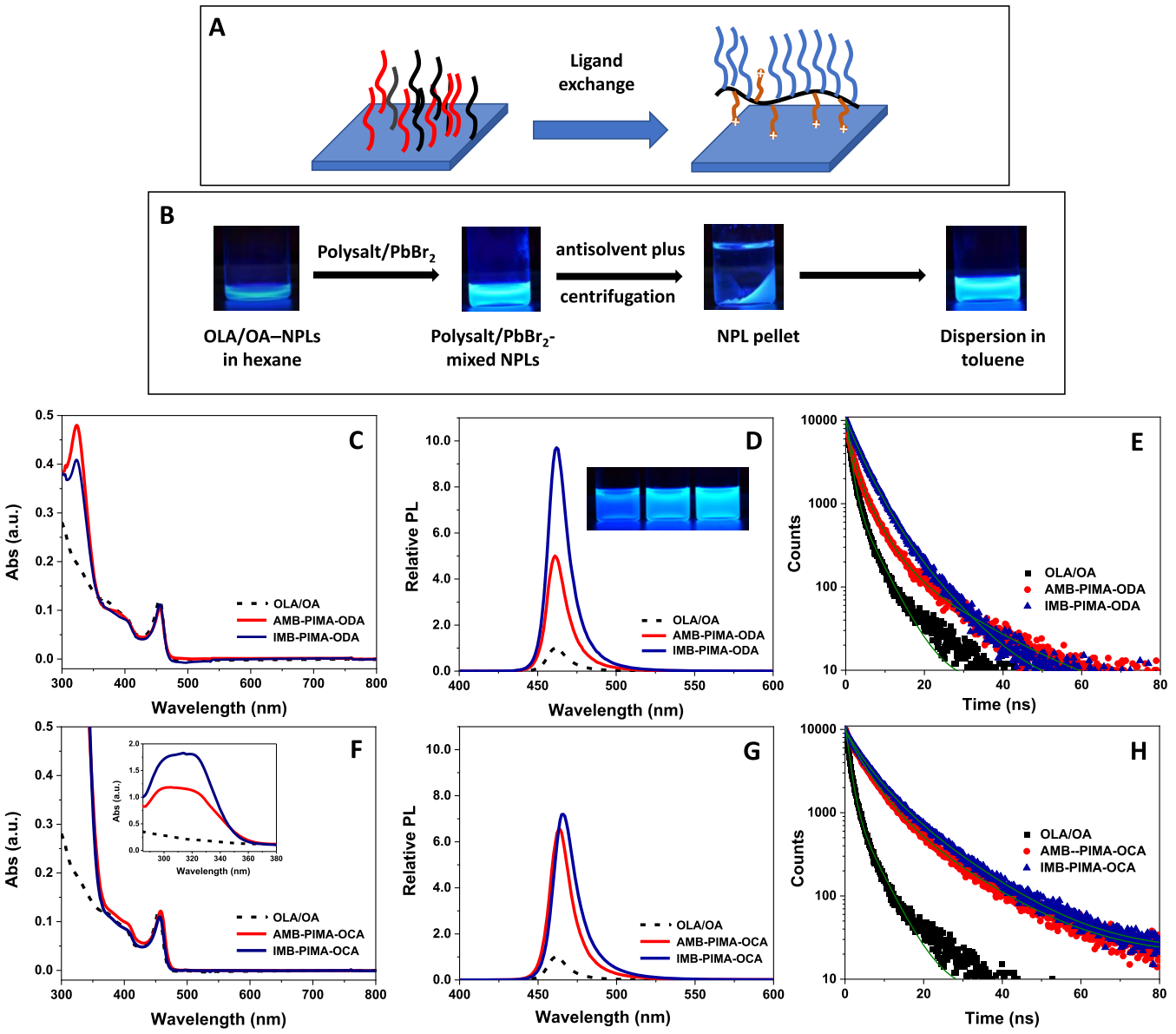

Figure 3. (A) Schematics of the ligand exchange process. (B) Steps of the substitution visualized under illumination using a hand-held UV lamp. (C) UV−vis absorption spectra of OLA/OA−, AMB-PIMA-ODA/$PbBr_2$− and IMB-PIMA-ODA/$PbBr_2$−NPLs in toluene. (D) Relative PL emission measured for the three sets of NPL dispersions (in panel C), reported with respect to the native, OLA/OA-coated materials. The inset shows fluorescence images of those dispersions. (E) PL lifetime decays of NPLs coated with either OLA/OA or the poly-ODA/$PbBr_2$ complexes. (F) Absorption spectra of the native NPLs and those coated with either AMB-PIMA-OCA/$PbBr_2$ or IMB-PIMA-OCA/$PbBr_2$ dispersed in THF. The inset shows the absorption peak of the $[Pb_xBr_y]^{2x-y}$ complex zoomed in the 290−380 nm range. (G) Relative PL spectra reported with respect to the intensity of OLA/OA−NPLs at λ_{max}. (H) PL lifetime decays measured before and after ligation with AMB-PIMA-OCA/$PbBr_2$ or IMB-PIMA-OCA/$PbBr_2$.

and from the as-grown materials are shown in Figure 3C. The spectra show a sharp first excitonic peak at ∼450 nm, indicating that the integrity of the NPLs has been preserved after ligand exchange. They also show one additional strong peak at ∼320 nm measured for the NPLs coated with polysalt/$PbBr_2$, which is attributed to the characteristic absorption band of the complex $[Pb_xBr_y]^{2x-y}$ anions. As shown in Figure 3D, all three NPLs show emission peaks centered at ∼460 nm with a full width at half maximum (FWHM) of ∼16 nm. The above optical features prove that the NPLs consist of three monolayers of $[PbBr_6]^{4-}$ octahedra and exhibit strong quantum confinement effects.[8,14,21,22,51] Interactions of the polysalt/$PbBr_2$ with the NPL surfaces promote a pronounced enhancement in the fluorescence intensity, without causing a shift in the emission profile. Indeed, we find that the as-grown NPLs only show a modest PLQY of ∼10%, attributed to the presence of a large number of defect states in the pristine materials.[14] In comparison, a substantially higher PL signal is measured for NPLs ligand exchanged with either AMB-PIMA-ODA/$PbBr_2$ or IMB-PIMA-ODA/$PbBr_2$ with a respective PLQY of 57% and 80% (see Table 1). We also carried out time-resolved PL (TR PL) measurements for all samples. The TR PL profiles acquired from the pristine NPLs are best fitted with a tri-exponential decay function with an average lifetime of ∼2.4 ns, whereas the average lifetime extracted for the polysalt/$PbBr_2$-ligated materials is ∼5.2 ns, see Figure 3E; note

https://doi.org/10.1021/acs.chemmater.2c00082
Chem. Mater. 2022, 34, 4924−4936

Table 1. Relative PL Intensity and Absolute PLQY Measured for NPLs with Different Coatings

NPL coating	relative PL intensity	absolute PLQY
OLA/OA	1	~10%
AMB-PIMA-ODA/$PbBr_2$	5.0	~57%
IMB-PIMA-ODA/$PbBr_2$	9.7	~80%
AMB-PIMA-OCA/$PbBr_2$	6.5	~63%
IMB-PIMA-OCA/$PbBr_2$	7.2	~65%

that the TR PL data exploited for the analysis were limited to the PL decaying region (i.e., without the initial rise) where the relevant information is deduced from. The longer exciton lifetime measured for the polymer-coated NPLs implies that the defect sites, which act as trap centers in the OLA/OA-stabilized materials, are better passivated with the polymer-complex ligands. This suppresses the nonradiative recombination channels and increases the PLQY. The fitting parameters deduced from the PL lifetime decay profiles (shown in Table 2) indicate that the short-lifetime component measured for the

Table 2. Components of the Lifetime (τ_i/Ns) Extracted from Fitting the PL Decay Profiles of NPLs with Different Coatings to a Tri-Exponential Function

NPL coating	$\tau_1(\alpha_1)$[a]	$\tau_2(\alpha_2)$	$\tau_3(\alpha_3)$	τ_{avg}[b]
OLA/OA	1.1 (0.43)	1.1 (0.43)	4.6 (0.13)	2.4 ns
AMB-PIMA-ODA/$PbBr_2$	1.2 (0.63)	3.9 (0.34)	15.3 (0.03)	5.2 ns
IMB-PIMA-ODA/$PbBr_2$	3.5 (0.41)	3.5 (0.41)	8.2 (0.18)	5.1 ns
AMB-PIMA-OCA/$PbBr_2$	1.2 (0.13)	3.5 (0.41)	13.7 (0.17)	8.3 ns
IMB-PIMA-OCA/$PbBr_2$	1.2 (0.07)	4.9 (0.65)	12.9 (0.28)	9.0 ns

[a] α_i's are amplitudes of the lifetime components. [b] τ_{avg} is defined as $\frac{\sum \alpha_i \tau_i^2}{\sum \alpha_i \tau_i}$.

as-grown samples has essentially disappeared from the profile fitting for the polymer−NPL samples, while the longer-lived components have larger contribution to the decay data. The poly-OCA/$PbBr_2$−NPLs dispersed in THF also exhibit significant PL enhancement and longer average lifetimes, as shown in Figure 3F−H. The PL enhancement and PLQY values measured for all NPLs with different coatings are summarized in Table 1, while the corresponding lifetime decay data are presented in Table 2.

Characterization of the Crystal Structure and Morphology of the Nanoplatelets. To understand whether or not the polysalt/$PbBr_2$ ligands alter the crystal structure of the NPLs, powder X-ray diffraction (PXRD) measurements were performed using both OLA/OA- and polymer-stabilized samples. The corresponding diffraction patterns are shown in Figure 4A. Owing to the preferential oriented stacking of anisotropic NPLs in a drop-cast film, the PXRD pattern of the native sample shows two dominant peaks at ~15.3° and ~30.8°.[52] The first can be unambiguously assigned to the diffraction of the (110) crystal plane in the orthorhombic phase, while the second one actually combines contributions of two close peaks ascribed to the (040) and (202) planes. These features confirm that an orthorhombic crystal structure characterizes the as-grown NPLs.[53,54] After ligand substitution with the polysalt/$PbBr_2$, the measured XRD patterns show weaker signals and broadened peaks. Overall, the diffraction patterns acquired for the various NPL samples (either OLA/OA-stabilized or coated with the polymers) match the one measured for the bulk $CsPbBr_3$ reference (ICSD 243735), which exhibits a Pnma orthorhombic phase.[53,54] It should be noted that reduction in the peak intensity combined with peak broadening of the modified NPL samples is likely due to a more random NPL orientation in the polymer-stabilized samples, compared to the starting materials. We also note that while the sample of the as-grown NPLs was formed by drop-casting the dispersion onto a substrate and letting dry, the polymer-stabilized NPL samples were prepared from dried precipitates.

To investigate potential changes in the morphological and structural properties of the $CsPbBr_3$ NPLs after ligand exchange, we employed high-angle annular dark-field scanning TEM (HAADF-STEM) measurements. Figure 4B,C show the TEM images collected from OLA/OA−NPLs under different magnifications. As we can see, most of the NPLs have a square shape with an average lateral size of ~9 ± 2.5 nm, and they lay flat on the TEM grid, an arrangement promoted during drying. The rather low contrast of the images may be attributed to the thin transversal dimension of the NPLs. A close inspection of the image shown in Figure 4B indicates the presence of a few small "islands" with much higher contrast, which are partially coalesced face-to-face-stacked NPLs into thicker nanosheets (see the higher magnification image in Figure 4H left panels). Such resolved structural arrangements enabled us to extract an estimate of the NPL thickness (~2 nm), which roughly corresponds to three monolayers of corner-sharing $[PbBr_6]^{4-}$ octahedra with a thickness of ~0.6 nm each.[14,21,55] This thickness is consistent with their absorption and emission, namely, a PL peak at ~460 nm. The images acquired from IMB-PIMA-ODA/$PbBr_2$−NPLs also show a large fraction of nanocrystals lying flat on the grid (see Figure 4D,E). Occasional corner etching of the square shape occurs, which makes the NPLs look like "disks". We note that for NPLs coated with IMB-PIMA-OCA/$PbBr_2$ and transferred to THF, porous structures can be identified in the TEM images, as shown in Figure 4F,G. These pores form during drying on the TEM grid and may be due to the more volatile THF and less favorable interactions between the polysalt and solvent.[56] Although less common, the TEM images acquired for the polysalt/$PbBr_2$-coated NPLs show a few upright stacked individual NPLs, which allow us to estimate the NPL thickness after ligand substitution (Figure 4H, right panels). Overall, both IMB-PIMA-ODA/$PbBr_2$- and IMB-PIMA-OCA/$PbBr_2$-stabilized NPLs preserve the square shape with an average lateral size of ~9 ± 3 nm and a thickness of ~2 nm. This result is very important because preserving the NPL thickness explains why the optical and spectroscopic features of the nanocrystals were unaltered after substitution with the polysalt/$PbBr_2$; the energy band gap is controlled by the strongly confined dimension (i.e., thickness) for perovskite NPLs. We found that OLA/OA-coated NPLs tend to coalesce on the TEM grid (see Figure S2). In contrast, the polymers provide additional benefits manifesting in the absence of large-scale coalescence of NPLs, which proves the ability of the ligands to preserve the morphological integrity of the starting materials. This is a very important observation with potential implications for use in optoelectronic devices.

Stability Tests. We now assess the stability of polymer-coated NPLs side-by-side with the native materials. Lack of long-term colloidal stability is one of the major limitations facing anisotropic $CsPbBr_3$ nanocrystals. OLA/OA−NPLs

https://doi.org/10.1021/acs.chemmater.2c00082
Chem. Mater. 2022, 34, 4924−4936

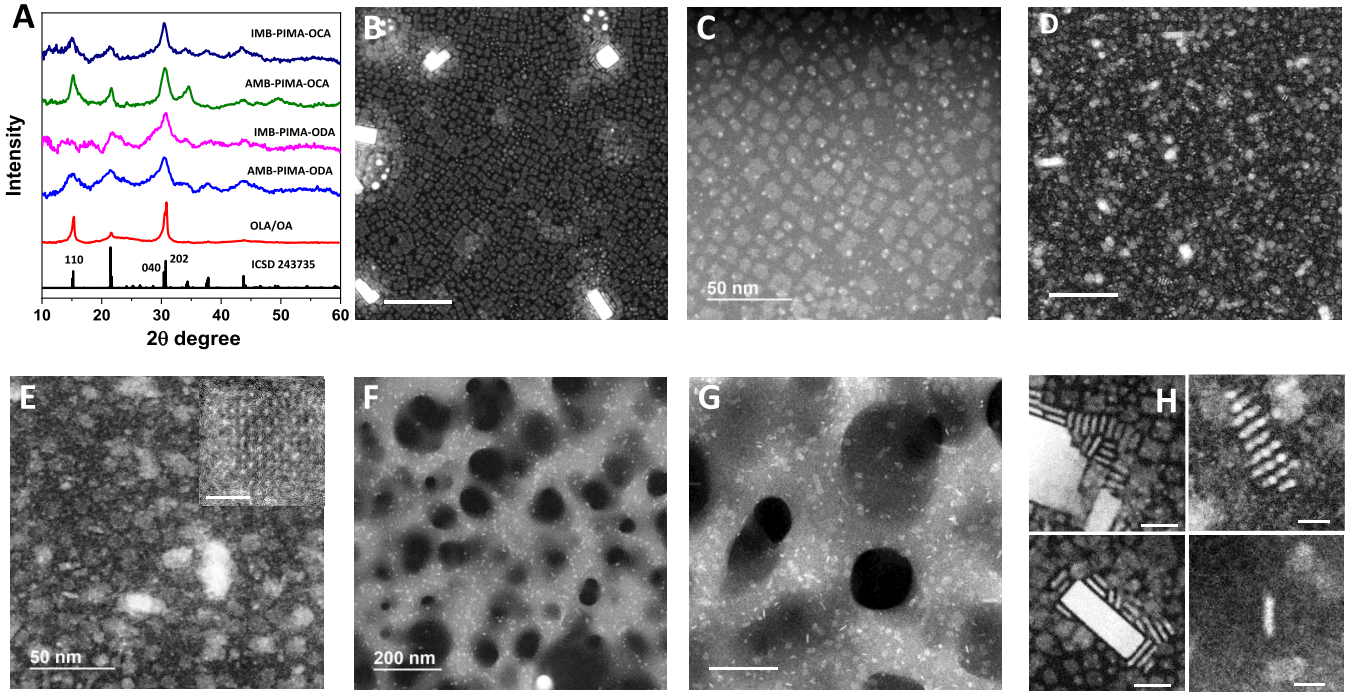

Figure 4. (A) Powder XRD patterns of OLA/OA-stabilized $CsPbBr_3$ NPLs together with those acquired after ligand substitution with the polysalt/$PbBr_2$ ligands. (B,C) HAADF-TEM images of OLA/OA−NPLs under different magnifications. (D,E) Images of IMB-PIMA-ODA/$PbBr_2$-capped NPLs. The inset in panel E is a high-resolution image showing resolved crystal planes in an individual nanocrystal. (F,G) Images of IMB-PIMA-OCA/$PbBr_2$-stabilized NPLs. (H) Representative high-magnification TEM images showing upright stacked NPLs: top left and bottom left images are acquired from OLA/OA−NPLs; top right and bottom right images correspond to IMB-PIMA-ODA/$PbBr_2$− and IMB-PIMA-OCA/$PbBr_2$−NPLs, respectively.

tend to undergo spontaneous aggregation and structural transformation within a few weeks, during storage under ambient conditions. This manifests in a progressive shift of the PL from blue to green, as shown in Figure S3, which can be attributed to a progressive morphological change from NPLs to nanocubes. We tracked the colloidal stability of the poly-ODA/$PbBr_2$−NPLs dispersed in toluene and poly-OCA/$PbBr_2$−NPLs dispersed in THF. Fluorescence images of different samples illuminated using a hand-held UV lamp were periodically acquired using a Nikon D3300 camera. Dispersions of both AMB-PIMA-ODA/$PbBr_2$- and IMB-PIMA-ODA/$PbBr_2$-capped NPLs stay homogenous and blue-emitting over a period of 2 months (see Figure 5A, left). The photoemission profiles measured for these dispersions are overall consistent with the fluorescent images, where a single PL peak centered at 460 nm is measured throughout the test period for the AMB/IMB-PIMA-ODA/$PbBr_2$-stabilized NPLs (see Figure 5B). However, when the NPLs are ligand-substituted with poly-OCA/$PbBr_2$ and dispersed in THF, they exhibit colloidal stability for ∼2 weeks (panel 5A, right). These results combined should be contrasted with data acquired for OLA/OA−NPLs; these dispersions lose their emission immediately after mixing with THF, a result attributed to destabilizing interactions with the solvent.

When used as color-generating/-converting materials in LEDs, perovskite nanostructures need to maintain strong and stable fluorescence emission. It is therefore critical to investigate the photostability of the surface-modified $CsPbBr_3$ NPLs. Here, we assessed the color stability of our NPL samples subjected to continuous UV radiation under ambient conditions. The PL spectra recorded from colloidal dispersions of OLA/OA−NPLs and IMB-PIMA-ODA/$PbBr_2$−NPLs under continuous UV radiation (4.5 W/cm^2) are shown in Figure 5C,D. Data collected from the native NPLs show that a single PL peak centered at ∼460 nm is initially measured, but a progressive change in the PL profile takes place during UV exposure, where a strong peak at 515 nm (green) builds up concomitant with reduction in the blue emission (at 460 nm), see Figure 5C. The inset in panel 5C shows that the emission of OLA/OA−NPLs shifts from blue to green with time under UV exposure. These results are consistent with previous findings, which reported that under sustained UV irradiation, OLA/OA−NPLs could undergo a morphological transformation to green-emitting nanostructures.[28,57] This morphological transformation was attributed to the fact that under UV irradiation, the weakly attached native ligands tend to experience higher rates of desorption from the NPL surfaces. This promotes ion migration and structural rearrangement of the surface atoms, leading to NPLs progressively morphing into more stable nanocubes. The process of ion diffusion and shape change is facilitated by the abundance of surface vacancies/defects in the native NPLs.[25,58] In contrast, IMB-PIMA-ODA/$PbBr_2$-coated NPLs generate a stable PL profile with a single sharp peak at ∼460 nm, even after UV exposure for 4 h, albeit with a decrease in the measured intensity (see Figure 5D). The measured difference in the PL data for the two sets of NPLs (as-grown and after coating with the polysalt/$PbBr_2$) was further complemented by tracking changes in the absorption profiles measured from these samples, see Figure S4. These results prove that the morphological transformation caused/facilitated by photo-induced high rates of ligand desorption and ion diffusion observed for the native materials are drastically reduced for polysalt/$PbBr_2$-stabilzed NPLs.

https://doi.org/10.1021/acs.chemmater.2c00082
Chem. Mater. 2022, 34, 4924−4936

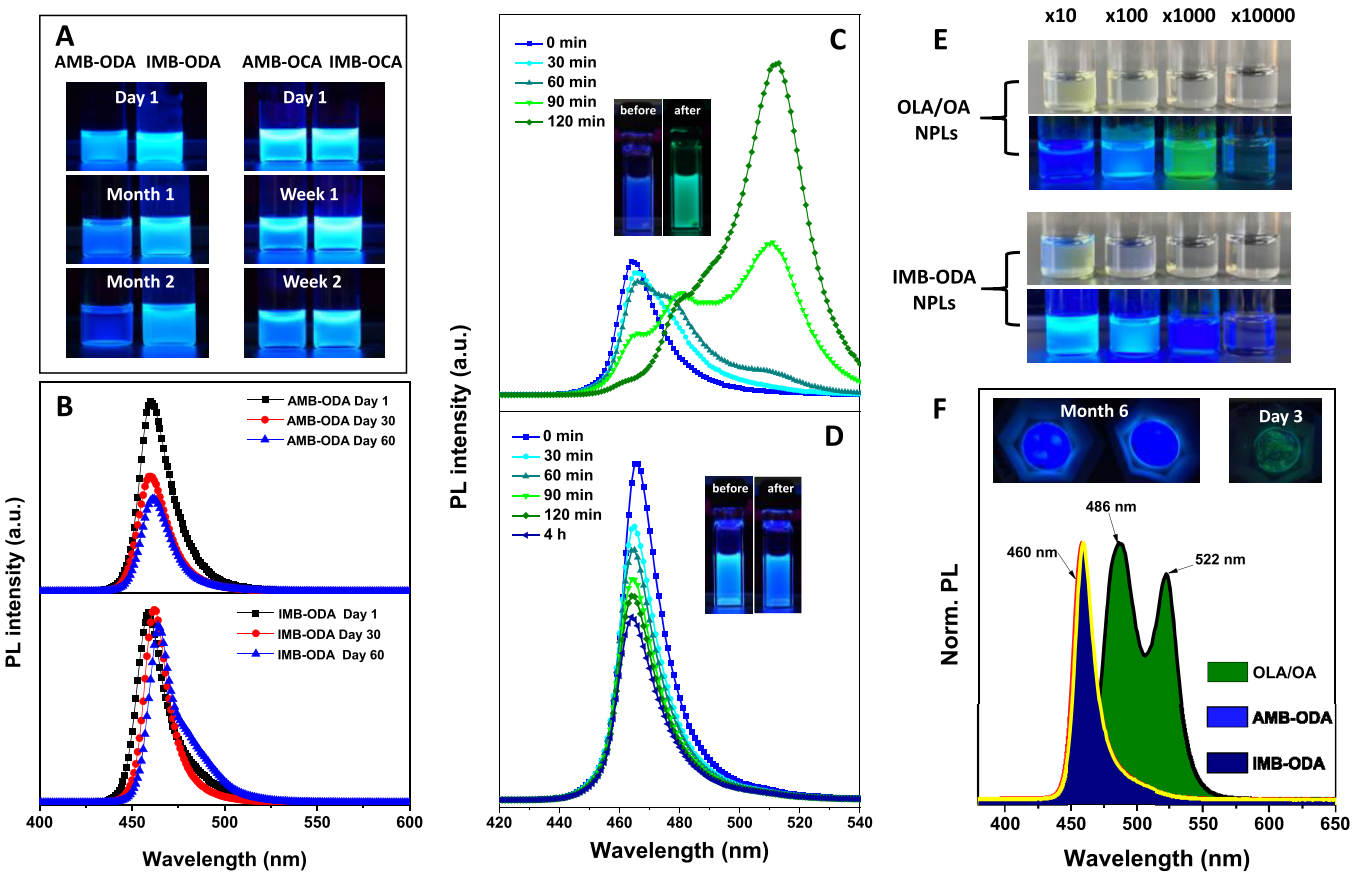

Figure 5. (A) Fluorescent images acquired from the polysalt/$PbBr_2$−NPL dispersions after storage at the indicated times. (B) Progression of the PL profile, over a 2-month storage period, for NPLs coated with AMB-PIMA-ODA/$PbBr_2$ (top) or IMB-PIMA-ODA/$PbBr_2$ (bottom) stored in toluene. (C,D) PL spectra of NPL dispersions tracked over different time periods while subjected to continuous UV irradiation under ambient conditions: (C) native OLA/OA−NPLs, (D) IMB-PIMA-ODA/$PbBr_2$−NPLs. (E) Dilution test applied to OLA/OA−NPLs and IMB-PIMA-ODA/$PbBr_2$−NPLs. (F) PL spectra collected from drop-cast films of OLA/OA−NPLs aged in air for 3 days, and AMB-PIMA-ODA/$PbBr_2$−NPLs or IMB-PIMA-ODA/$PbBr_2$−NPLs aged in air for 6 months. The inset in panel F shows the fluorescence images of the films: polymer-stabilized NPLs (left) and OLA/OA-capped NPLs (right).

High dilution tests were also applied to both OLA/OA−NPLs and IMB-PIMA-ODA/$PbBr_2$−NPLs to further evaluate the colloidal stability of the polymer-coated NPLs. This test can be used to assess if the newly introduced ligands exhibit strong or weak binding to the NC surfaces. As demonstrated by Alivisatos and co-workers, weakly binding ligands can easily desorb from the NC surfaces under highly diluted conditions, which tends to create halide vacancies and reduce ligand density.[32,33,59] This in turn lowers the rate of radiative recombination and eventually induces aggregation buildup in the sample. This issue is particularly severe for anisotropic NPLs with their high energy surfaces. The dilution test results shown in Figure 5E demonstrate that under 100-fold dilution, the pristine NPLs undergo a rapid aggregation and loss of blue emission, indicating a loss of NPL integrity and colloidal stability. In contrast, NPLs coated with IMB-PIMA-ODA/$PbBr_2$ exhibit much better stability under similar dilution conditions. There is no aggregation or shift of emission even under 1000-fold dilution (see Figure S5). Clearly, the polysalt/$PbBr_2$ coating provides substantially enhanced binding affinity to the NPL surfaces, which prevents the loss of colloidal and morphological stability under highly diluted conditions.

In addition to solution stability tests, we also investigated the behavior of polymer-stabilized materials in thin film structures (solid state), given the importance of these sample conditions for device applications. For this, thin films of OLA/OA−, AMB-PIMA-ODA/$PbBr_2$− and IMB-PIMA-ODA/$PbBr_2$−NPLs were prepared by drop-casting dispersions of these materials in toluene onto glass slides and letting them dry. These films were then tracked to monitor their photophysical stability with time. We found that films of OLA/OA−NPLs exhibited morphological changes where loss of film homogeneity along with shift of the PL to green emission took place after 3 days of storage under ambient conditions (see panel 5F, right inset). This color change reflects the buildup of a dual emission signal with peaks centered at ∼486 nm and ∼520 nm, as shown in Figure 5F. In comparison, films of the polymer-stabilized NPLs maintained their homogeneous morphology and blue color purity for at least 6 months of storage (see panel 5F and left inset). Additionally, we found that pure blue emission was preserved for powder samples of the polysalt/$PbBr_2$-stabilized NPLs for up to 9 months of storage under ambient conditions (see Figure S6). Retention of blue color emission in dry films and powder samples of the polymer-stabilized NPLs proves that the anisotropic quantum-confined nanoplatelets stayed intact during extended storage. This constitutes a major achievement of the introduced surface treatment strategy.

Insights into the Effect of Ligand-Plus-Salt Combination. Clearly, the above results prove that mixing $PbBr_2$ with

https://doi.org/10.1021/acs.chemmater.2c00082
Chem. Mater. 2022, 34, 4924−4936

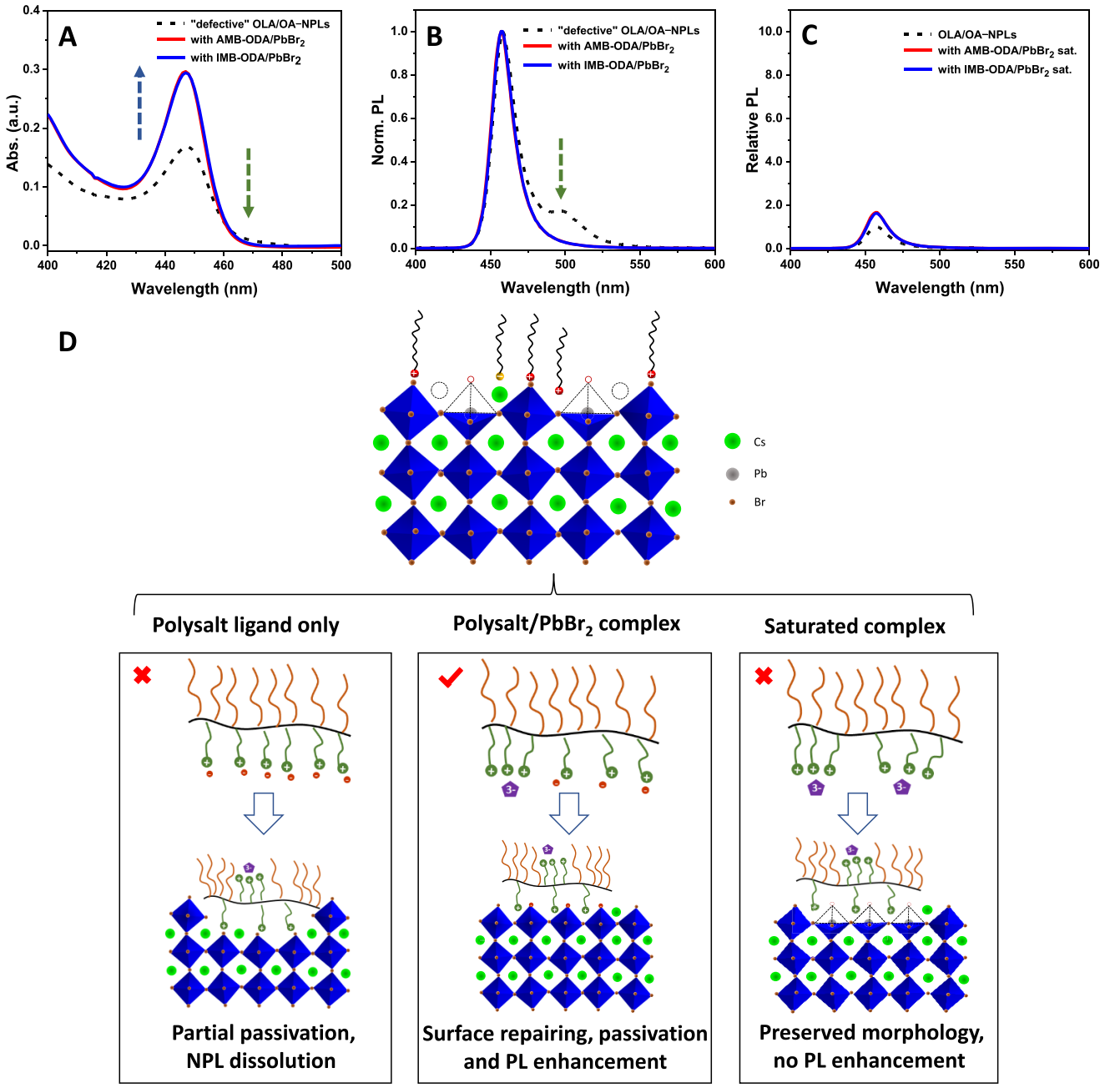

Figure 6. (A) Absorption and (B) normalized PL profiles of "defective" OLA/OA–NPLs and those passivated by polysalt/$PbBr_2$ dispersed in toluene. (C) Side-by-side comparison of the PL acquired from as-grown materials and those passivated by polysalt/$PbBr_2$ complex under saturated conditions. (D) Proposed model explaining mechanistically the interactions between the polysalt/$PbBr_2$ complex and the NPL surfaces: (left) polysalt alone, (middle) polysalt/$PbBr_2$ complex below saturation conditions in toluene, and (right) polysalt/$PbBr_2$ complex under saturated conditions in toluene.

the polysalt plays an important role in improving the colloidal and morphological stability, in addition to providing electronic passivation of the NPL surfaces. In contrast, mixing the native nanocrystals with the polysalt ligands alone induces progressive destabilization of the NPLs and the appearance of a new absorption feature at ~320–325 nm. The absorption feature corresponds to the buildup of new salt species made of ligand complexed with either $[Pb_4Br_{11}]^{3-}$ anions in toluene, or ligand complexed with a mixture of $[Pb_4Br_{11}]^{3-}$ and $[PbBr_3]^-$ anions in THF (see Figure 2).[39] Ligand substitution using polysalt/$PbBr_2$ prevents NPL dissolution even when high molar equivalents of the ligand complexes are added. However, a few lingering questions remain, including what does the inclusion of $PbBr_2$ complex add to the polysalt coating of the NPLs, and how does that improve the photophysical properties of the resulting materials?

To gain further insights into the mechanistic effects of the salt, we have conducted two simple experiments. In the first, we identified a heterogeneous growth dispersion that contains a fraction of defective NPLs; note that preparing inhomogeneous NPL samples is not highly unusual, given the difficulty to control the fast growth kinetics of perovskite nanocrystals.[16,22,54,60,61] For such sample, we are able to identify a low-energy tail in the absorption and emission profiles, in addition

https://doi.org/10.1021/acs.chemmater.2c00082
Chem. Mater. 2022, 34, 4924–4936

to the dominant excitonic peak at 450 nm and main PL peak at 460 nm (see Figure 6A,B, dashed lines). We have found that mixing the as-grown dispersion with a poly-ODA/$PbBr_2$ complex solution in toluene immediately eliminated the low-energy tail and simultaneously increased the intensity of the excitonic peak at 450 nm. Concomitantly, we measured an emission profile without a low-energy shoulder, but enhanced PL intensity (Figure 6A,B). These changes unequivocally prove that using the poly-ODA/$PbBr_2$ complex (as ligands) promotes homogenization of the NPL population in a dispersion. In the second experiment, we attempted to identify the anion species responsible for the PL enhancement, focusing on toluene samples, namely, is it $[Pb_4Br_{11}]^{3-}$ or $[Br]^-$? For this, we mixed the OLA/OA−NPLs with a polysalt/complex in toluene (using polysalt:$PbBr_2$ = 1:4, i.e., large excess of $PbBr_2$). This reduces the concentration of free $[Br]^-$ in the medium because of the large equilibrium constant and sufficient stability of $[Pb_4Br_{11}]^{3-}$.[39] We found that under these conditions, the measured PL enhancement was rather modest (∼1.5−2 times at most), compared to those measured for samples mixed with unsaturated polysalt/$PbBr_2$ or even polysalt ligand only (compare data in Figures 1C and 3D,G to those in Figure 6C). Long-term colloidal stability can still be achieved under these conditions, nonetheless.

We now propose a mechanistic model, which implies that two types of interactions control the polysalt/$PbBr_2$-promoted stabilization of the nanoplatelets, schematically shown in Figure 6D. One involves electrostatic interactions between the ammonium (or imidazolium) cations and the NPL surface, by filling the Cs^+ sites, which promotes stronger coordination interactions because of the chelation effect, and better long-term colloidal stability. The other involves repairing bromide vacancies, which ultimately requires the presence of free $[Br]^-$ anions in the medium. The concentration of $[Br]^-$ depends on the complex species generated upon the addition of $PbBr_2$ to the ligand solution. Figure 6D shows that below saturation conditions, charge neutrality requires a lower concentration of $[Pb_4Br_{11}]^{3-}$ mixed with $[Br]^-$ in toluene. Conversely, for solutions in THF, interaction with the polymer produces monovalent and trivalent complexes ($[PbBr_3]^-$ and $[Pb_4Br_{11}]^{3-}$) along with the native $[Br]^-$. In both configurations, the soluble Br^- anions play a key role in repairing surface vacancies, although the process is more efficient in the presence of $[Pb_4Br_{11}]^{3-}$ (i.e., in toluene dispersions). Overall, interactions of the polysalt/$PbBr_2$ with the as-grown materials promote more stable coating, given the multidentate nature of the polymer binding, with several ammonium or imidazolium groups filling vacated Cs^+ sites, together with ligand-mediated reconstruction of defective NPLs; this can be viewed as a "size-focusing" promoted by the coordinating ligands.[62,63] This interpretation is also consistent with previous reports, which proposed that halide vacancies are the predominant source of trap states in perovskite nanocrystals.[15,33] Here, we anticipate that the ammonium/imidazolium cations in the polymer and $[PbBr_3]^-$/$[Pb_4Br_{11}]^{3-}$ anions do not play a direct role in repairing defects, but they would interact with the NPL surfaces and act as stabilizing organic−inorganic ligands. This proposal is consistent with the fact that NPLs coated with $PbBr_2$-saturated polysalts also exhibit good colloidal stability combined with an unchanged PL emission.

CONCLUSIONS

We have shown that surface treatment of 2D $CsPbBr_3$ nanoplatelets with a solution of polysalt/$PbBr_2$ complex (as ligands) successfully achieves colloidal and morphological stabilization of these anisotropic nanostructures. Furthermore, the treatment promotes electronic passivation, yielding NPLs with significantly enhanced PL, where QYs up to ∼80% have been recorded. Powder X-ray diffraction and TEM characterizations confirm that the polymer-coated NPLs preserve their core crystal structure and morphology. Various stability tests applied to the surface-modified NPLs confirm that our strategy yields materials with significantly enhanced colloidal stability, where the anisotropic morphology and deep blue emission under various conditions are maintained. These include stability against UV irradiation and under highly diluted conditions. The polymer-stabilized materials dried in thin films and as powder also preserve their blue fluorescence during extended storage. Additional experiments starting with rather defective NPL samples, which exhibit low-energy tails in the absorption and emission profiles, have allowed us to gain mechanistic understanding for the polysalt/$PbBr_2$ interactions with the NPLs. We have found that treatment of such dispersions with unsaturated polysalt/$PbBr_2$ increased the optical density of the sample and completely eliminated the low-energy tails, yielding homogeneous dispersions with enhanced fluorescence. However, modest PL enhancement but good colloidal and morphological stability have been realized in the presence of saturated polysalt/$PbBr_2$; these results are attributed to the preservation of the anisotropic morphology of the NPLs. These findings combined clearly highlight the importance of devising effective surface chemistry to control the stability and fluorescence properties of 2D perovskite NPLs. They also allow us to conclude that the species responsible for the enhanced PLQY are mainly free $[Br]^-$ ions in the medium, not $[Pb_xBr_y]^{2x-y}$ or ammonium cations. The resulting NPLs are greatly promising for use in blue light-emitting devices, where drastic limitations traced to low QY and lack of blue color purity have affected currently tested materials. Finally, we anticipate that the present polymer-complex design, combined with additional chemical tuning of the cations and anions involved, will yield ligands that can potentially passivate other lead halide perovskite quantum dots and nanoplatelets, such as iodide-based compounds.

EXPERIMENTAL SECTION

Growth of $CsPbBr_3$ Nanoplatelets. Growth of the NPLs was carried out using the method reported by Bohn and coworkers, but a few minor adjustments were implemented to accommodate a larger-scale reaction.[14] The Cs-oleate precursor was prepared by reacting Cs_2CO_3 (0.1 mmol, 32.6 mg) with 10 mL of OA with heating at 80 °C until full dissolution of the white powder. The $PbBr_2$ precursor solution was prepared by dissolving $PbBr_2$ (0.5 mmol, 183.5 mg) in 50 mL of toluene containing a mixture of 500 μL of OA and 500 μL of oleylamine, under continuous stirring while heating at 80 °C. Complete dissolution of the salt in toluene under these conditions requires ∼2 h. The growth of NPLs was carried out under room temperature conditions. Briefly, Cs-oleate (500 μL) was added to the toluene solution containing the $PbBr_2$ precursor (5 mL), yielding a yellowish clear solution. After ∼1 min of stirring, 6 mL of acetone was rapidly added to initiate growth of the NPLs. The solution was initially clear, and then gradually became turbid. Growth was complete after 5 min of stirring under these conditions. The mixture was then centrifuged at 3600 rpm for 10 min, the supernatant was

https://doi.org/10.1021/acs.chemmater.2c00082
Chem. Mater. 2022, 34, 4924−4936

discarded, and the precipitate was redispersed in 4 mL of hexane and stored for further experiments and characterization. Overall, similar concentrations of NPL dispersions were used. Typically, a stock dispersion has an optical density at 400 nm (measured in a 0.5 cm optical path length cell) of ~0.18−0.2, after 50-fold dilution.

Preparation of the Polysalt/$PbBr_2$ Complex. When preparing the polysalt/$PbBr_2$ complex, the molar ratio between $PbBr_2$ and salt groups in the polymer is critically important. The molar ratio of added $PbBr_2$ to salt groups in the polysalt chain used in the present experiments is ~0.7:1, that is, conditions allowing a partial complexation of the ammonium or imidazolium groups along the backbone.

Synthesis of the ODA-Based Polysalt/$PbBr_2$ Complex. First, 40 mg (~0.02 mmol anchors) of AMB-PIMA-ODA or IMB-PIMA-ODA, prepared following previous protocols, was dissolved in 2 mL of toluene using a 10 mL scintillation vial.[35] Then, 5 mg of $PbBr_2$ was added to the solution, followed by stirring at 60 °C until full dissolution of the salt (~30 min). After cooling the mixture to room temperature, a small amount of precipitate was formed, which might be associated with the formation of $L[PbBr_4]$ that is insoluble in organic solvents. These precipitates were removed by centrifugation, and the supernatant containing a solution of the poly-ODA/$PbBr_2$ was retrieved and used in ligand substitution experiments.

Synthesis of the OCA-Based Polysalt/$PbBr_2$ Complex. AMB-PIMA-OCA or IMB-PIMA-OCA (30 mg, ~0.02 mmol anchors) was loaded in a 10 mL scintillation vial.[35] Then, 4 mL of THF was added to dissolve the polysalt. To the resulting clear solution, $PbBr_2$ (5 mg, 0.0136 mmol) was added, followed by sonication for 5 min until the salt was fully dissolved. The polysalt-only solution has a very weak blue emission, but after reacting with $PbBr_2$, the solution exhibited red emission (under UV excitation), indicating the formation of $[PbBr_3]^-$. It should be noted that a small amount of white precipitate forms in the solution, which can be removed by centrifugation. The collected supernatant solution of the poly-OCA/$PbBr_2$ complex was used for further experiments.

Ligand Exchange. *Ligand Exchange with AMB/IMB-PIMA-ODA/$PbBr_2$.* As-grown $CsPbBr_3$ NPLs (200 μL) dispersed in hexane were transferred to a 7 mL scintillation vial. The polysalt-ODA/$PbBr_2$ complex (400 μL) (~8 mg AMB-PIMA-ODA or IMB-PIMA-ODA in toluene) prepared above was added, and the mixture was sonicated for 2 min. Then, 4 mL of ethyl acetate was added to precipitate the NPLs. After centrifugation at 4000 rpm for 5 min, the supernatant was discarded, and the precipitate was redispersed in 400 μL of toluene. The polymer-ligated NPL dispersions were used as stock solution for further characterization; we note that after ligand substitution, the new stock dispersion in toluene has a smaller NPL concentration, ~1/2 of the starting OLA/OA-stabilized NPLs in hexane. Also, the ligand exchange can be scaled up by 10 times, without altering the quality of the obtained materials.

Ligand Exchange with AMB/IMB-PIMA-OCA/$PbBr_2$. As-grown $CsPbBr_3$ NPLs (200 μL) in hexane were loaded into a 7 mL scintillation vial, and then, 800 μL of polysalt-OCA/$PbBr_2$ complex (~6 mg of ligand) solution was added. An immediate color change of the solution mixture visible under room light was recorded. After sonication for 2 min, 2 mL of ethyl acetate was added, producing a turbid mixture, indicating precipitation of the surface-modified NPLs. Then, one round of centrifugation (3500 rpm, 5 min) was applied, the clear supernatant was discarded, and the precipitate containing the NPLs was dispersed in 400 μL of THF for further characterization.

■ ASSOCIATED CONTENT

Supporting Information

The Supporting Information is available free of charge at https://pubs.acs.org/doi/10.1021/acs.chemmater.2c00082.

Additional information, materials, instrumentation, absorption and PL data of salt complexes, polysalt/$PbBr_2$-passivated nanoplatelets, TEM images of as-grown NPLs, colloidal and photophysical stability tests under diluted conditions, and stability in thin film structures (PDF)

■ AUTHOR INFORMATION

Corresponding Author

Hedi Mattoussi − *Department of Chemistry and Biochemistry, Florida State University, Tallahassee, Florida 32306, United States;* orcid.org/0000-0002-6511-9323; Email: mattoussi@chem.fsu.edu

Authors

Sisi Wang − *Department of Chemistry and Biochemistry, Florida State University, Tallahassee, Florida 32306, United States*

Wentao Wang − *Department of Chemistry and Biochemistry, Florida State University, Tallahassee, Florida 32306, United States;* orcid.org/0000-0003-2273-4171

Selin Donmez − *Department of Chemistry and Biochemistry, Florida State University, Tallahassee, Florida 32306, United States;* orcid.org/0000-0002-1377-2689

Yan Xin − *National High Magnetic Field Laboratory, Florida State University, Tallahassee, Florida 32310, United States*

Complete contact information is available at: https://pubs.acs.org/10.1021/acs.chemmater.2c00082

Notes

The authors declare no competing financial interest.

■ ACKNOWLEDGMENTS

The authors thank FSU and the National Science Foundation (NSF-CHE, Grant Nos. #1508501 and #2005079), AFOSR (Grant No. FA9550-18-1-0144) and Kasei-Asahi Corporation for financial support. TEM experiments were performed at the National High Magnetic Field Laboratory, which is supported by National Science Foundation Cooperative Agreement No. DMR-1644779 and the State of Florida (Grant No. FA9550-18-1-0144).

■ REFERENCES

(1) Kagan, C. R.; Lifshitz, E.; Sargent, E. H.; Talapin, D. V. Building devices from colloidal quantum dots. *Science* **2016**, *353*, No. aac5523.

(2) Liu, Y.; Cui, J.; Du, K.; Tian, H.; He, Z.; Zhou, Q.; Yang, Z.; Deng, Y.; Chen, D.; Zuo, X.; Ren, Y.; Wang, L.; Zhu, H.; Zhao, B.; Di, D.; Wang, J.; Friend, R. H.; Jin, Y. Efficient blue light-emitting diodes based on quantum-confined bromide perovskite nanostructures. *Nat. Photonics* **2019**, *13*, 760−764.

(3) Yuan, S.; Cui, L.-S.; Dai, L.; Liu, Y.; Liu, Q.-W.; Sun, Y.-Q.; Auras, F.; Anaya, M.; Zheng, X.; Ruggeri, E.; Yu, Y.-J.; Qu, Y.-K.; Abdi-Jalebi, M.; Bakr, O. M.; Wang, Z.-K.; Stranks, S. D.; Greenham, N. C.; Liao, L.-S.; Friend, R. H. Efficient and Spectrally Stable Blue Perovskite Light-Emitting Diodes Employing a Cationic π-Conjugated Polymer. *Adv. Mater.* **2021**, *33*, No. 2103640.

(4) Worku, M.; Ben-Akacha, A.; Sridhar, S.; Frick, J. R.; Yin, S.; He, Q.; Robb, A. J.; Chaaban, M.; Liu, H.; Winfred, J. S. R. V.; Hanson, K.; So, F.; Dougherty, D.; Ma, B. Band Edge Control of Quasi-2D Metal Halide Perovskites for Blue Light-Emitting Diodes with Enhanced Performance. *Adv. Funct. Mater.* **2021**, *31*, No. 2103299.

(5) Kovalenko, M. V.; Protesescu, L.; Bodnarchuk, M. I. Properties and potential optoelectronic applications of lead halide perovskite nanocrystals. *Science* **2017**, *358*, 745−750.

(6) Dong, Y.; Wang, Y.-K.; Yuan, F.; Johnston, A.; Liu, Y.; Ma, D.; Choi, M.-J.; Chen, B.; Chekini, M.; Baek, S.-W.; Sagar, L. K.; Fan, J.; Hou, Y.; Wu, M.; Lee, S.; Sun, B.; Hoogland, S.; Quintero-Bermudez, R.; Ebe, H.; Todorovic, P.; Dinic, F.; Li, P.; Kung, H. T.; Saidaminov, M. I.; Kumacheva, E.; Spiecker, E.; Liao, L.-S.; Voznyy, O.; Lu, Z.-H.;

Sargent, E. H. Bipolar-shell resurfacing for blue LEDs based on strongly confined perovskite quantum dots. *Nat. Nanotechnol.* **2020**, *15*, 668−674.
(7) Dey, A.; Ye, J.; De, A.; Debroye, E.; Ha, S. K.; Bladt, E.; Kshirsagar, A. S.; Wang, Z.; Yin, J.; Wang, Y.; Quan, L. N.; Yan, F.; Gao, M.; Li, X.; Shamsi, J.; Debnath, T.; Cao, M.; Scheel, M. A.; Kumar, S.; Steele, J. A.; Gerhard, M.; Chouhan, L.; Xu, K.; Wu, X.-G.; Li, Y.; Zhang, Y.; Dutta, A.; Han, C.; Vincon, I.; Rogach, A. L.; Nag, A.; Samanta, A.; Korgel, B. A.; Shih, C.-J.; Gamelin, D. R.; Son, D. H.; Zeng, H.; Zhong, H.; Sun, H.; Demir, H. V.; Scheblykin, I. G.; Mora-Seró, I.; Stolarczyk, J. K.; Zhang, J. Z.; Feldmann, J.; Hofkens, J.; Luther, J. M.; Pérez-Prieto, J.; Li, L.; Manna, L.; Bodnarchuk, M. I.; Kovalenko, M. V.; Roeffaers, M. B. J.; Pradhan, N.; Mohammed, O. F.; Bakr, O. M.; Yang, P.; Müller-Buschbaum, P.; Kamat, P. V.; Bao, Q.; Zhang, Q.; Krahne, R.; Galian, R. E.; Stranks, S. D.; Bals, S.; Biju, V.; Tisdale, W. A.; Yan, Y.; Hoye, R. L. Z.; Polavarapu, L. State of the Art and Prospects for Halide Perovskite Nanocrystals. *ACS Nano* **2021**, *15*, 10775−10981.
(8) Otero-Martínez, C.; Ye, J.; Sung, J.; Pastoriza-Santos, I.; Pérez-Juste, J.; Xia, Z.; Rao, A.; Hoye, R. L. Z.; Polavarapu, L. Colloidal Metal-Halide Perovskite Nanoplatelets: Thickness-Controlled Synthesis, Properties, and Application in Light-Emitting Diodes. *Adv. Mater.* **2022**, *34*, No. 2107105.
(9) Chiba, T.; Hayashi, Y.; Ebe, H.; Hoshi, K.; Sato, J.; Sato, S.; Pu, Y.-J.; Ohisa, S.; Kido, J. Anion-exchange red perovskite quantum dots with ammonium iodine salts for highly efficient light-emitting devices. *Nat. Photonics* **2018**, *12*, 681−687.
(10) Kim, Y.-H.; Kim, S.; Kakekhani, A.; Park, J.; Park, J.; Lee, Y.-H.; Xu, H.; Nagane, S.; Wexler, R. B.; Kim, D.-H.; Jo, S. H.; Martínez-Sarti, L.; Tan, P.; Sadhanala, A.; Park, G.-S.; Kim, Y.-W.; Hu, B.; Bolink, H. J.; Yoo, S.; Friend, R. H.; Rappe, A. M.; Lee, T.-W. Comprehensive defect suppression in perovskite nanocrystals for high-efficiency light-emitting diodes. *Nat. Photonics* **2021**, *15*, 148−155.
(11) Hou, S.; Gangishetty, M. K.; Quan, Q.; Congreve, D. N. Efficient Blue and White Perovskite Light-Emitting Diodes via Manganese Doping. *Joule* **2018**, *2*, 2421−2433.
(12) Lignos, I.; Protesescu, L.; Emiroglu, D. B.; Maceiczyk, R.; Schneider, S.; Kovalenko, M. V.; deMello, A. J. Unveiling the Shape Evolution and Halide-Ion-Segregation in Blue-Emitting Formamidinium Lead Halide Perovskite Nanocrystals Using an Automated Microfluidic Platform. *Nano Lett.* **2018**, *18*, 1246−1252.
(13) Zhang, H.; Fu, X.; Tang, Y.; Wang, H.; Zhang, C.; Yu, W. W.; Wang, X.; Zhang, Y.; Xiao, M. Phase segregation due to ion migration in all-inorganic mixed-halide perovskite nanocrystals. *Nat. Commun.* **2019**, *10*, 1088.
(14) Bohn, B. J.; Tong, Y.; Gramlich, M.; Lai, M. L.; Döblinger, M.; Wang, K.; Hoye, R. L. Z.; Müller-Buschbaum, P.; Stranks, S. D.; Urban, A. S.; Polavarapu, L.; Feldmann, J. Boosting Tunable Blue Luminescence of Halide Perovskite Nanoplatelets through Post-synthetic Surface Trap Repair. *Nano Lett.* **2018**, *18*, 5231−5238.
(15) Wu, Y.; Wei, C.; Li, X.; Li, Y.; Qiu, S.; Shen, W.; Cai, B.; Sun, Z.; Yang, D.; Deng, Z.; Zeng, H. In Situ Passivation of PbBr64− Octahedra toward Blue Luminescent $CsPbBr_3$ Nanoplatelets with Near 100% Absolute Quantum Yield. *ACS Energy Lett.* **2018**, *3*, 2030−2037.
(16) Xiao, X.; Li, Y.; Xie, R.-J. Blue-emitting and self-assembled thinner perovskite CsPbBr3 nanoplates: synthesis and formation mechanism. *Nanoscale* **2020**, *12*, 9231−9239.
(17) Zheng, X.; Hou, Y.; Sun, H.-T.; Mohammed, O. F.; Sargent, E. H.; Bakr, O. M. Reducing Defects in Halide Perovskite Nanocrystals for Light-Emitting Applications. *J. Phys. Chem. Lett.* **2019**, *10*, 2629−2640.
(18) Zhang, B.-B.; Yuan, S.; Ma, J.-P.; Zhou, Y.; Hou, J.; Chen, X.; Zheng, W.; Shen, H.; Wang, X.-C.; Sun, B.; Bakr, O. M.; Liao, L.-S.; Sun, H.-T. General Mild Reaction Creates Highly Luminescent Organic-Ligand-Lacking Halide Perovskite Nanocrystals for Efficient Light-Emitting Diodes. *J. Am. Chem. Soc.* **2019**, *141*, 15423−15432.
(19) Hoye, R. L. Z.; Lai, M.-L.; Anaya, M.; Tong, Y.; Gałkowski, K.; Doherty, T.; Li, W.; Huq, T. N.; Mackowski, S.; Polavarapu, L.; Feldmann, J.; MacManus-Driscoll, J. L.; Friend, R. H.; Urban, A. S.; Stranks, S. D. Identifying and Reducing Interfacial Losses to Enhance Color-Pure Electroluminescence in Blue-Emitting Perovskite Nanoplatelet Light-Emitting Diodes. *ACS Energy Lett.* **2019**, *4*, 1181−1188.
(20) Almeida, G.; Goldoni, L.; Akkerman, Q.; Dang, Z.; Khan, A. H.; Marras, S.; Moreels, I.; Manna, L. Role of Acid−Base Equilibria in the Size, Shape, and Phase Control of Cesium Lead Bromide Nanocrystals. *ACS Nano* **2018**, *12*, 1704−1711.
(21) Akkerman, Q. A.; Motti, S. G.; Srimath Kandada, A. R.; Mosconi, E.; D'Innocenzo, V.; Bertoni, G.; Marras, S.; Kamino, B. A.; Miranda, L.; De Angelis, F.; Petrozza, A.; Prato, M.; Manna, L. Solution Synthesis Approach to Colloidal Cesium Lead Halide Perovskite Nanoplatelets with Monolayer-Level Thickness Control. *J. Am. Chem. Soc.* **2016**, *138*, 1010−1016.
(22) Bekenstein, Y.; Koscher, B. A.; Eaton, S. W.; Yang, P.; Alivisatos, A. P. Highly Luminescent Colloidal Nanoplates of Perovskite Cesium Lead Halide and Their Oriented Assemblies. *J. Am. Chem. Soc.* **2015**, *137*, 16008−16011.
(23) De Roo, J.; Ibáñez, M.; Geiregat, P.; Nedelcu, G.; Walravens, W.; Maes, J.; Martins, J. C.; Van Driessche, I.; Kovalenko, M. V.; Hens, Z. Highly Dynamic Ligand Binding and Light Absorption Coefficient of Cesium Lead Bromide Perovskite Nanocrystals. *ACS Nano* **2016**, *10*, 2071−2081.
(24) Smock, S. R.; Chen, Y.; Rossini, A. J.; Brutchey, R. L. The Surface Chemistry and Structure of Colloidal Lead Halide Perovskite Nanocrystals. *Acc. Chem. Res.* **2021**, *54*, 707−718.
(25) Wang, Y.; Li, X.; Sreejith, S.; Cao, F.; Wang, Z.; Stuparu, M. C.; Zeng, H.; Sun, H. Photon Driven Transformation of Cesium Lead Halide Perovskites from Few-Monolayer Nanoplatelets to Bulk Phase. *Adv. Mater.* **2016**, *28*, 10637−10643.
(26) Dang, Z.; Dhanabalan, B.; Castelli, A.; Dhall, R.; Bustillo, K. C.; Marchelli, D.; Spirito, D.; Petralanda, U.; Shamsi, J.; Manna, L.; Krahne, R.; Arciniegas, M. P. Temperature-Driven Transformation of $CsPbBr_3$ Nanoplatelets into Mosaic Nanotiles in Solution through Self-Assembly. *Nano Lett.* **2020**, *20*, 1808−1818.
(27) Zhang, C.; Wan, Q.; Wang, B.; Zheng, W.; Liu, M.; Zhang, Q.; Kong, L.; Li, L. Surface Ligand Engineering toward Brightly Luminescent and Stable Cesium Lead Halide Perovskite Nanoplatelets for Efficient Blue-Light-Emitting Diodes. *J. Phys. Chem. C* **2019**, *123*, 26161−26169.
(28) Shamsi, J.; Kubicki, D.; Anaya, M.; Liu, Y.; Ji, K.; Frohna, K.; Grey, C. P.; Friend, R. H.; Stranks, S. D. Stable Hexylphosphonate-Capped Blue-Emitting Quantum-Confined $CsPbBr_3$ Nanoplatelets. *ACS Energy Lett.* **2020**, *5*, 1900−1907.
(29) Peng, S.; Wen, Z.; Ye, T.; Xiao, X.; Wang, K.; Xia, J.; Sun, J.; Zhang, T.; Mei, G.; Liu, H.; Xu, B.; Li, X.; Chen, R.; Xing, G.; Wang, K.; Tang, Z. Effective Surface Ligand-Concentration Tuning of Deep-Blue Luminescent $FAPbBr_3$ Nanoplatelets with Enhanced Stability and Charge Transport. *ACS Appl. Mater. Interfaces* **2020**, *12*, 31863−31874.
(30) Pan, J.; Quan, L. N.; Zhao, Y.; Peng, W.; Murali, B.; Sarmah, S. P.; Yuan, M.; Sinatra, L.; Alyami, N. M.; Liu, J.; Yassitepe, E.; Yang, Z.; Voznyy, O.; Comin, R.; Hedhili, M. N.; Mohammed, O. F.; Lu, Z. H.; Kim, D. H.; Sargent, E. H.; Bakr, O. M. Highly Efficient Perovskite-Quantum-Dot Light-Emitting Diodes by Surface Engineering. *Adv. Mater.* **2016**, *28*, 8718−8725.
(31) Krieg, F.; Ochsenbein, S. T.; Yakunin, S.; ten Brinck, S.; Aellen, P.; Süess, A.; Clerc, B.; Guggisberg, D.; Nazarenko, O.; Shynkarenko, Y.; Kumar, S.; Shih, C.-J.; Infante, I.; Kovalenko, M. V. Colloidal $CsPbX_3$ (X = Cl, Br, I) Nanocrystals 2.0: Zwitterionic Capping Ligands for Improved Durability and Stability. *ACS Energy Lett.* **2018**, *3*, 641−646.
(32) Zhang, B.; Goldoni, L.; Zito, J.; Dang, Z.; Almeida, G.; Zaccaria, F.; de Wit, J.; Infante, I.; De Trizio, L.; Manna, L. Alkyl Phosphonic Acids Deliver $CsPbBr_3$ Nanocrystals with High Photoluminescence Quantum Yield and Truncated Octahedron Shape. *Chem. Mater.* **2019**, *31*, 9140−9147.

https://doi.org/10.1021/acs.chemmater.2c00082
Chem. Mater. 2022, 34, 4924−4936

(33) Nenon, D. P.; Pressler, K.; Kang, J.; Koscher, B. A.; Olshansky, J. H.; Osowiecki, W. T.; Koc, M. A.; Wang, L.-W.; Alivisatos, A. P. Design Principles for Trap-Free $CsPbX_3$ Nanocrystals: Enumerating and Eliminating Surface Halide Vacancies with Softer Lewis Bases. *J. Am. Chem. Soc.* **2018**, *140*, 17760−17772.
(34) Wang, S.; Du, L.; Jin, Z.; Xin, Y.; Mattoussi, H. Enhanced Stabilization and Easy Phase Transfer of $CsPbBr_3$ Perovskite Quantum Dots Promoted by High-Affinity Polyzwitterionic Ligands. *J. Am. Chem. Soc.* **2020**, *142*, 12669−12680.
(35) Wang, S.; Du, L.; Donmez, S.; Xin, Y.; Mattoussi, H. Polysalt ligands achieve higher quantum yield and improved colloidal stability for $CsPbBr_3$ quantum dots. *Nanoscale* **2021**, *13*, 16705−16718.
(36) Jin, Z.; Du, L.; Zhang, C.; Sugiyama, Y.; Wang, W.; Palui, G.; Wang, S.; Mattoussi, H. Modification of Poly(maleic anhydride)-Based Polymers with H2N−R Nucleophiles: Addition or Substitution Reaction? *Bioconjugate Chem.* **2019**, *30*, 871−880.
(37) Wang, W.; Ji, X.; Kapur, A.; Zhang, C.; Mattoussi, H. A Multifunctional Polymer Combining the Imidazole and Zwitterion Motifs as a Biocompatible Compact Coating for Quantum Dots. *J. Am. Chem. Soc.* **2015**, *137*, 14158−14172.
(38) Wang, W.; Kapur, A.; Ji, X.; Safi, M.; Palui, G.; Palomo, V.; Dawson, P. E.; Mattoussi, H. Photoligation of an Amphiphilic Polymer with Mixed Coordination Provides Compact and Reactive Quantum Dots. *J. Am. Chem. Soc.* **2015**, *137*, 5438−5451.
(39) Jones, A. R.; Aikens, D. A. The nature of pb(II)-bromide complexes in propylene carbonate. *Polyhedron* **1982**, *1*, 169−174.
(40) Balakrishnan, S. K.; Kamat, P. V. Ligand Assisted Transformation of Cubic $CsPbBr_3$ Nanocrystals into Two-Dimensional $CsPb_2Br_5$ Nanosheets. *Chem. Mater.* **2018**, *30*, 74−78.
(41) Bodnarchuk, M. I.; Boehme, S. C.; ten Brinck, S.; Bernasconi, C.; Shynkarenko, Y.; Krieg, F.; Widmer, R.; Aeschlimann, B.; Günther, D.; Kovalenko, M. V.; Infante, I. Rationalizing and Controlling the Surface Structure and Electronic Passivation of Cesium Lead Halide Nanocrystals. *ACS Energy Lett.* **2019**, *4*, 63−74.
(42) Imran, M.; Ijaz, P.; Goldoni, L.; Maggioni, D.; Petralanda, U.; Prato, M.; Almeida, G.; Infante, I.; Manna, L. Simultaneous Cationic and Anionic Ligand Exchange For Colloidally Stable $CsPbBr_3$ Nanocrystals. *ACS Energy Lett.* **2019**, *4*, 819−824.
(43) Abiodun, S. L.; Gee, M. Y.; Greytak, A. B. Combined NMR and Isothermal Titration Calorimetry Investigation Resolves Conditions for Ligand Exchange and Phase Transformation in $CsPbBr_3$ Nanocrystals. *J. Phys. Chem. C* **2021**, *125*, 17897−17905.
(44) Quarta, D.; Imran, M.; Capodilupo, A.-L.; Petralanda, U.; van Beek, B.; De Angelis, F.; Manna, L.; Infante, I.; De Trizio, L.; Giansante, C. Stable Ligand Coordination at the Surface of Colloidal $CsPbBr_3$ Nanocrystals. *J. Phys. Chem. Lett.* **2019**, *10*, 3715−3726.
(45) Song, J.; Fang, T.; Li, J.; Xu, L.; Zhang, F.; Han, B.; Shan, Q.; Zeng, H. Organic−Inorganic Hybrid Passivation Enables Perovskite QLEDs with an EQE of 16.48%. *Adv. Mater.* **2018**, *30*, No. 1805409.
(46) Chiba, T.; Takahashi, Y.; Sato, J.; Ishikawa, S.; Ebe, H.; Tamura, K.; Ohisa, S.; Kido, J. Surface Crystal Growth of Perovskite Nanocrystals via Postsynthetic Lead(II) Bromide Treatment to Increase the Colloidal Stability and Efficiency of Light-Emitting Devices. *ACS Appl. Mater. Interfaces* **2020**, *12*, 45574−45581.
(47) Stamplecoskie, K. G.; Manser, J. S.; Kamat, P. V. Dual nature of the excited state in organic−inorganic lead halide perovskites. *Energy Environ. Sci.* **2015**, *8*, 208−215.
(48) Yoon, S. J.; Stamplecoskie, K. G.; Kamat, P. V. How Lead Halide Complex Chemistry Dictates the Composition of Mixed Halide Perovskites. *J. Phys. Chem. Lett.* **2016**, *7*, 1368−1373.
(49) Oldenburg, K.; Vogler, A. Electronic Spectra and Photochemistry of Tin(II), Lead(II), Antimony(III), and Bismuth(III) Bromide Complexes in Solution. *Z. Naturforsch. B* **1993**, *48*, 1519−1523.
(50) Dohner, E. R.; Hoke, E. T.; Karunadasa, H. I. Self-Assembly of Broadband White-Light Emitters. *J. Am. Chem. Soc.* **2014**, *136*, 1718−1721.
(51) Yang, D.; Zou, Y.; Li, P.; Liu, Q.; Wu, L.; Hu, H.; Xu, Y.; Sun, B.; Zhang, Q.; Lee, S.-T. Large-scale synthesis of ultrathin cesium lead bromide perovskite nanoplates with precisely tunable dimensions and their application in blue light-emitting diodes. *Nano Energy* **2018**, *47*, 235−242.
(52) Bertolotti, F.; Nedelcu, G.; Vivani, A.; Cervellino, A.; Masciocchi, N.; Guagliardi, A.; Kovalenko, M. V. Crystal Structure, Morphology, and Surface Termination of Cyan-Emissive, Six-Monolayers-Thick $CsPbBr_3$ Nanoplatelets from X-ray Total Scattering. *ACS Nano* **2019**, *13*, 14294−14307.
(53) Shamsi, J.; Dang, Z.; Bianchini, P.; Canale, C.; Di Stasio, F.; Brescia, R.; Prato, M.; Manna, L. Colloidal Synthesis of Quantum Confined Single Crystal CsPbBr3 Nanosheets with Lateral Size Control up to the Micrometer Range. *J. Am. Chem. Soc.* **2016**, *138*, 7240−7243.
(54) Liang, Z.; Zhao, S.; Xu, Z.; Qiao, B.; Song, P.; Gao, D.; Xu, X. Shape-Controlled Synthesis of All-Inorganic $CsPbBr_3$ Perovskite Nanocrystals with Bright Blue Emission. *ACS Appl. Mater. Interfaces* **2016**, *8*, 28824−28830.
(55) Sun, S.; Yuan, D.; Xu, Y.; Wang, A.; Deng, Z. Ligand-Mediated Synthesis of Shape-Controlled Cesium Lead Halide Perovskite Nanocrystals via Reprecipitation Process at Room Temperature. *ACS Nano* **2016**, *10*, 3648−3657.
(56) Bui, V.-T.; Dao, V.-D.; Choi, H.-S. Transferable thin films with sponge-like porous structure via improved phase separation. *Polymer* **2016**, *101*, 184−191.
(57) Shamsi, J.; Rastogi, P.; Caligiuri, V.; Abdelhady, A. L.; Spirito, D.; Manna, L.; Krahne, R. Bright-Emitting Perovskite Films by Large-Scale Synthesis and Photoinduced Solid-State Transformation of $CsPbBr_3$ Nanoplatelets. *ACS Nano* **2017**, *11*, 10206−10213.
(58) Liu, J.; Song, K.; Shin, Y.; Liu, X.; Chen, J.; Yao, K. X.; Pan, J.; Yang, C.; Yin, J.; Xu, L.-J.; Yang, H.; El-Zohry, A. M.; Xin, B.; Mitra, S.; Hedhili, M. N.; Roqan, I. S.; Mohammed, O. F.; Han, Y.; Bakr, O. M. Light-Induced Self-Assembly of Cubic CsPbBr3 Perovskite Nanocrystals into Nanowires. *Chem. Mater.* **2019**, *31*, 6642−6649.
(59) Krieg, F.; Ong, Q. K.; Burian, M.; Rainò, G.; Naumenko, D.; Amenitsch, H.; Süess, A.; Grotevent, M. J.; Krumeich, F.; Bodnarchuk, M. I.; Shorubalko, I.; Stellacci, F.; Kovalenko, M. V. Stable Ultraconcentrated and Ultradilute Colloids of CsPbX3 (X = Cl, Br) Nanocrystals Using Natural Lecithin as a Capping Ligand. *J. Am. Chem. Soc.* **2019**, *141*, 19839−19849.
(60) Ravi, V. K.; Swarnkar, A.; Chakraborty, R.; Nag, A. Excellent green but less impressive blue luminescence from CsPbBr3perovskite nanocubes and nanoplatelets. *Nanotechnology* **2016**, *27*, No. 325708.
(61) Lv, L.; Xu, Y.; Fang, H.; Luo, W.; Xu, F.; Liu, L.; Wang, B.; Zhang, X.; Yang, D.; Hu, W.; Dong, A. Generalized colloidal synthesis of high-quality, two-dimensional cesium lead halide perovskite nanosheets and their applications in photodetectors. *Nanoscale* **2016**, *8*, 13589−13596.
(62) Razgoniaeva, N.; Yang, M.; Garrett, P.; Kholmicheva, N.; Moroz, P.; Eckard, H.; Royo Romero, L.; Porotnikov, D.; Khon, D.; Zamkov, M. Just Add Ligands: Self-Sustained Size Focusing of Colloidal Semiconductor Nanocrystals. *Chem. Mater.* **2018**, *30*, 1391−1398.
(63) Shimpi, J. R.; Sidhaye, D. S.; Prasad, B. L. V. Digestive Ripening: A Fine Chemical Machining Process on the Nanoscale. *Langmuir* **2017**, *33*, 9491−9507.

https://doi.org/10.1021/acs.chemmater.2c00082
Chem. Mater. 2022, 34, 4924−4936